Achieving Highly Efficient, Selective, and Stable CO_2 Reduction on Nitrogen-Doped Carbon Nanotubes

Jingjie Wu,[†] Ram Manohar Yadav,[†] Mingjie Liu,[†] Pranav P. Sharma,[‡] Chandra Sekhar Tiwary,[§] Lulu Ma,[†] Xiaolong Zou,[†] Xiao-Dong Zhou,[*,‡] Boris I. Yakobson,[†] Jun Lou,[*,†] and Pulickel M. Ajayan[*,†]

[†]Department of Material Science and NanoEngineering, Rice University, Houston, Texas 77005, United States, [‡]Department of Chemical Engineering, University of South Carolina, Columbia, South Carolina 29201, United States, and [§]Department of Materials Engineering, Indian Institute of Science, Bangalore 560012, India

ABSTRACT The challenge in the electrosynthesis of fuels from CO_2 is to achieve durable and active performance with cost-effective catalysts. Here, we report that carbon nanotubes (CNTs), doped with nitrogen to form resident electron-rich defects, can act as highly efficient and, more importantly, stable catalysts for the conversion of CO_2 to CO. The unprecedented overpotential (−0.18 V) and selectivity (80%) observed on nitrogen-doped CNTs (NCNTs) are attributed to their unique features to facilitate the reaction, including (i) high electrical conductivity, (ii) preferable catalytic sites (pyridinic N defects), and (iii) low free energy for CO_2 activation and high barrier for hydrogen evolution. Indeed, DFT calculations show a low free energy barrier for the potential-limiting step to form key intermediate COOH as well as strong binding energy of adsorbed COOH and weak binding energy for the adsorbed CO. The highest selective site toward CO production is pyridinic N, and the NCNT-based electrodes exhibit no degradation over 10 h of continuous operation, suggesting the structural stability of the electrode.

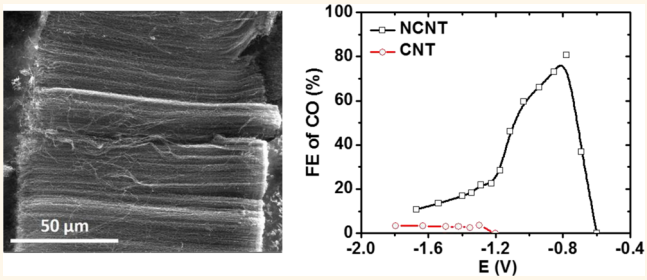

KEYWORDS: carbon nanotubes · pyridinic nitrogen · CO_2 reduction · low overpotential · high selectivity · high durability

Mastery of the electrochemical conversion of carbon dioxide and water to fuels using renewable electricity has the potential to shed light on understanding the nature of artificial photosynthesis and offer an approach to mitigate the negative impact of anthropogenic carbon dioxide emissions on the planet.[1−4] The field, however, has not substantially advanced in the last 30 years primarily because of the challenge of discovery of chemically active and structurally stable electrocatalysts and membrane architectures. An ideal catalyst for the electroreduction of CO_2, *e.g.*, $CO_2 + 2H^+ + 2e^- \rightarrow CO + H_2O$, is capable of mediating proton-coupled electron transfer, possessing a low overpotential for CO_2 activation while being sluggish toward hydrogen evolution, exhibiting a preferable selectivity toward a target product, and retaining structural integrity over a long operation. Significant progress has been made since 2011[2,5,6] toward addressing the chemical activity originated from the oxide scale or tuned ionic-liquid/catalyst interfaces. Silver and gold can selectively convert CO_2 to CO, a feedstock for the synthesis of methanol in the Fischer−Tropsch process,[1,5] while the ionic liquid can function as a co-catalyst to lower the overpotential and subsequently improve the reaction kinetics. Copper and tin are known nonprecious metallic catalysts. Copper is found to be active toward the formation of hydrogen carbon and alcohols.[2,7−9] Tin exhibits a superior selectivity toward the formation of formate with a Faradaic efficiency up to 98%.[3] A rapid performance degradation was observed in both Sn- and Cu-based electrodes after approximately 30 min from the start of CO_2 electrolysis.[2,10−12] As a result, it is compelling to search for efficient, durable, and inexpensive alternatives to metal electrocatalysts for CO_2 conversion.

Nitrogen-doped carbon nanotubes (NCNTs) are known to be an effective electrocatalyst for the oxygen reduction reaction (ORR). The activity of a NCNT catalyst originates from its local defects that mediate the electronic

* Address correspondence to zhox@cec.sc.edu, jlou@rice.edu, ajayan@rice.edu.

Received for review February 15, 2015 and accepted April 21, 2015.

Published online April 21, 2015
10.1021/acsnano.5b01079

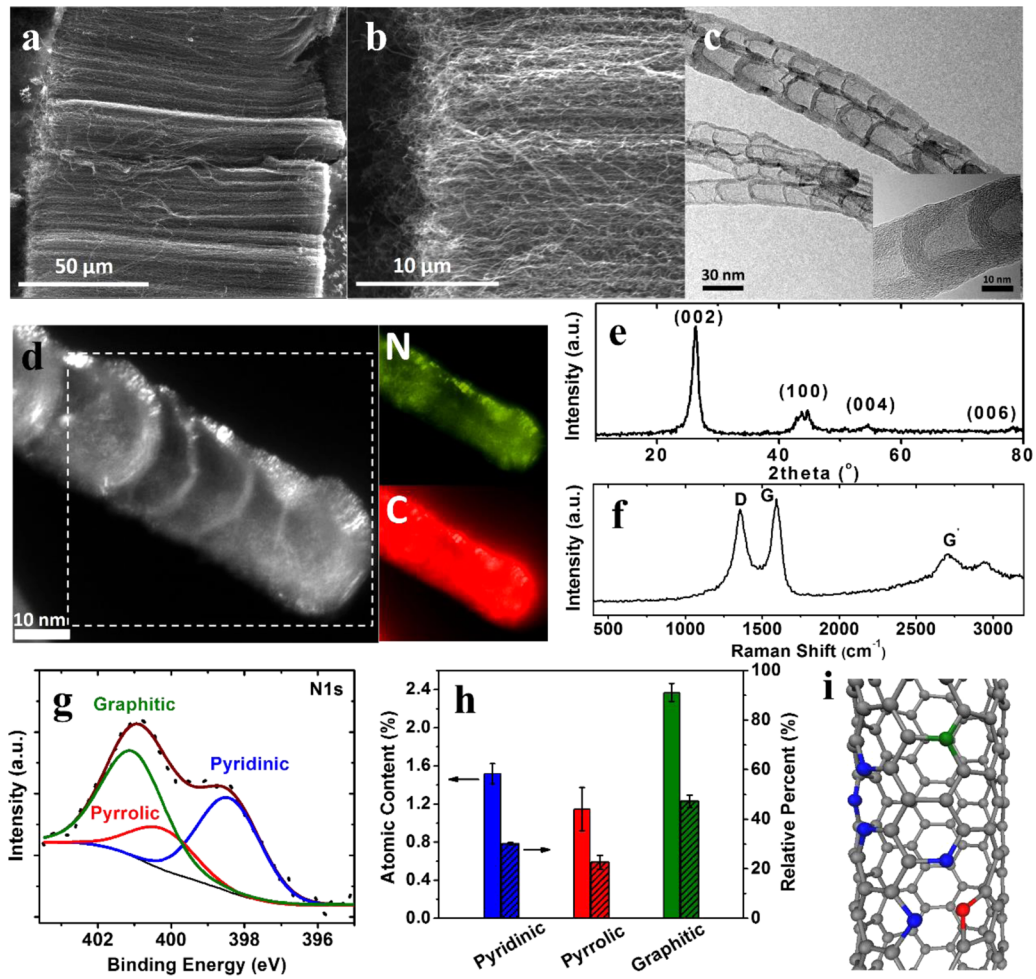

Figure 1. Physical characterization of NCNTs. (a, b) SEM images of NCNTs at low and high magnification, respectively. (c) TEM images of NCNTs (inset shows a single multiwall NCNT). (d) EELS element mapping of N and C. (e) XRD pattern. (f) Raman spectrum. (g) Representative XPS of N 1s for NCNTs. The N 1s is deconvoluted into three peaks representing three different N functionalities. (h) Statistic N atomic content and relative percent. (i) Schematic of graphitic, pyrrolic, and pyridinic N configuration.

structure[13,14] and its surface morphology that regulates atomic arrangement and coordination.[14] So far, there are very limited reports on the use of CNTs or NCNTs as the catalyst for the electroreduction of CO_2. CNTs have been applied as the support for the catalytically active species rather than a catalyst itself.[15,16] NCNTs with a modification of polyethylenimine were found to function as a catalyst to reduce CO_2 to formate but at a high overpotential.[17] The activity of NCNTs toward the reduction of CO_2 remains largely unknown. The aim of this paper is to report our recent investigation on the use of NCNTs as the catalysts for the direct conversion of CO_2 to fuel with an unprecedented low overpotential (−0.18 V), high selectivity (80%), and durability.

RESULTS AND DISCUSSION

The NCNTs were synthesized by the liquid chemical vapor deposition (CVD) method, injecting liquid precursor acetonitrile and dicyandiamide with ferrocene in Ar/H_2 atmosphere at 850 °C. Spraying of the precursor solution leads to a homogeneous NCNT deposition along the heating zone inside the quartz tube. The scanning electron microscope (SEM) investigation reveals the formation of well-aligned NCNT arrays (Figure 1a, b). Transmission electron microscope (TEM) analysis explores the details of the microstructure where the NCNTs are multiwalled with a bamboo- shaped morphology due to nitrogen incorporation and free from amorphous and vitreous carbon (Figure 1c and inset). The mean tube diameter is around 30 nm (Supporting Information, Figure S1). The electron energy loss spectroscopy (EELS) elemental mapping shows homogeneous N distribution in the single NCNT (Figure 1d).

In addition to morphology, the structural characterizations were performed by X-ray diffraction (XRD) and Raman spectroscopy. The sharpness of the (002) peak shows the high crystallinity and graphetic nature of NCNTs (Figure 1e). The Raman spectrum shows a strong G-band at around 1584 cm^{-1} and a D-band at around 1355 cm^{-1} (Figure 1f). The intensity ratio of the D to G modes (I_d/I_g) for our NCNTs is 0.87, which increases as compared to that of pristine CNT ($I_d/I_g = 0.58$,

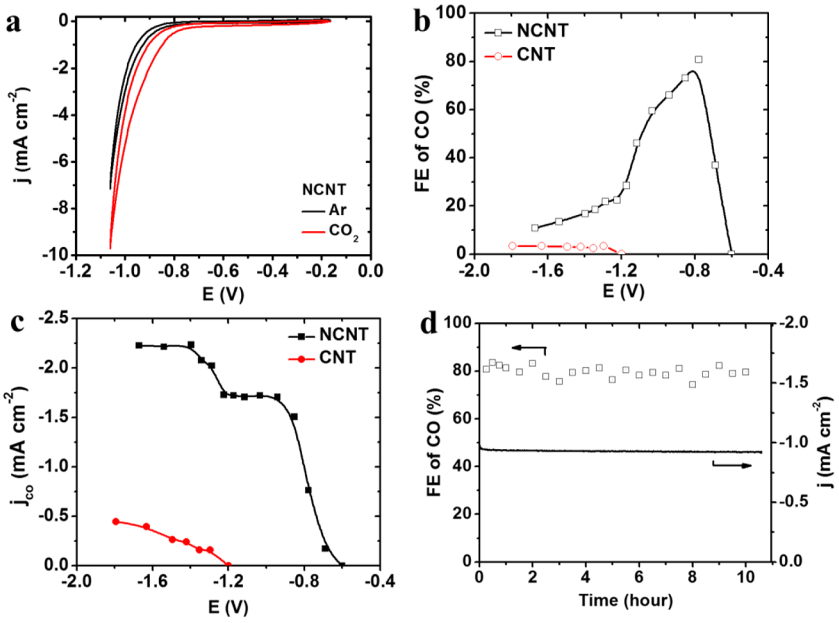

Figure 2. Performance of NCNTs for selectively electrochemical reduction of CO_2 to CO. (a) CVs for NCNTs in Ar- and CO_2-saturated 0.1 M $KHCO_3$ electrolyte, 50 mV s^{-1}. (b) Dependence of FE of CO on applied cell potential during electrocatalysis of CO_2 reduction for both NCNTs and CNTs catalysts. (c) Partial current density of CO *versus* applied cell potential for NCNTs and CNTs catalysts. (d) Stability of performance of NCNTs for CO_2 reduction operated at potentiostatic mode of −0.8 V for 10 h. Both current density and FE of CO remain steady over the duration of the test.

Supporting Information, Figure S9) due to nitrogen incorporation.[18] The doping of nitrogen in carbon nanotubes leads to local distortion in graphitic sheets due to differences in atomic masses and chemical bond lengths of carbon and nitrogen and thus is responsible for the increase in the I_d/I_g ratio for NCNTs as compared to pristine CNTs.

The atomic configuration and stoichiometric composition of NCNTs were analyzed by X-ray photoelectron spectroscopy (XPS). The total N atomic content [N/(C + N)] in the NCNTs calculated from the integrated peak area under the C 1s and N 1s signal divided by their atomic sensitivity factor is approximately 5.0 atom % (Supporting Information, Figure S2). The high-resolution N 1s spectrum as shown in Figure 1g deconvolutes into subpeaks at around 398.5, 400.8, and 401.5 eV, revealing three N configurations in the carbon sp^2 network corresponding to pyridinic, pyrrolic, and graphitic N, respectively, as shown in the schematic (Figure 1i). The graphitic N has the highest relative concentration followed by pyridinic and pyrrolic N. The individual atomic content for pyridinic, pyrrolic and graphitic N is 1.5, 1.1, and 2.4 atom %, respectively (Figure 1h).

The activity of NCNTs toward the electrocatalytic reduction of CO_2 was evaluated in a full electrochemical cell employing a circulating electrolyte of 0.1 M $KHCO_3$ as shown in our previous work.[19] A catalyst ink was prepared from the NCNTs mixing with Nafion dispersion, 2-propanol, and deionized water and then sprayed onto carbon paper with a diffusion layer to form a gas diffusion electrode (GDE). The NCNT GDE was inserted into the full electrochemical cell and served as the cathodic electrode for CO_2 reduction. The anodic electrode was Pt/C for H_2 oxidation; therefore, the overpotential loss in the anode is negligible (Supporting Information, Figure S3).

The cyclic voltammetry (CV) curves of NCNTs acquired in Ar-saturated 0.1 M $KHCO_3$ show the onset potential of −0.82 V for the hydrogen evolution reaction (HER), which indicates high overpotential (−0.41 V) with reference to the apparent standard cell potential (−0.41 V under pH = 7 for 0.1 M KOH) for HER (Figure 2a). The suppression of HER on NCNTs is beneficial for CO_2 reduction. When the gas supply is replaced with CO_2, the reduction current increases significantly. This increment in reduction current indicates some CO_2 reduction reaction in addition to the HER. The change in reduction current, however, is not conclusive evidence for CO_2 reduction since the hydrogen evolution and CO_2 reduction are often interconnected, and CO_2 dissolving in the electrolyte will in turn lower the pH to further enhance the HER. Consequently, the reduction products were monitored under potentiostatic electrolysis to further confirm the occurrence of CO_2 reduction. During the electrolysis of CO_2, the cathodic compartment of the cell was continuously purged with CO_2 gas and vented directly into the sampling loop of a gas chromatography to enable the quantification of the gas phase products. The liquid-phase products were measured by ^1H nuclear magnetic resonance (NMR) after electrolysis at each potential. NCNTs exhibit activity to the exclusive formation of CO while no liquid product is detected by NMR throughout the applied cell potential range.

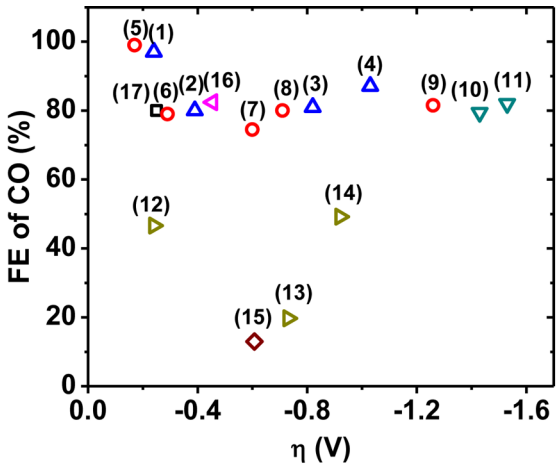

No.	Symbol	Catalyst	Electrolyte	Ref.
1	△	Oxide-derived Au	0.5 $NaKCO_3$	1
2	△	Polycrystalline Au foil	0.5 $NaKCO_3$	1
3	△	Au powder (800 nm)	0.1 $KHCO_3$	This work
4	△	Polycrystalline Au foil	0.1 $KHCO_3$	25
5	○	Ag powder (100 nm)	EMIMBF4	5
6	○	Nanoporous Ag	0.5 $KHCO_3$	26
7	○	Ag particles (20-40 nm)	0.1 $KHCO_3$	This work
8	○	Ag powder (1 μm)	0.1 $KHCO_3$	27
9	○	Polycrystalline Ag foil	0.1 $KHCO_3$	2
10	▽	Zn powder (100 nm)	0.1 $KHCO_3$	This work
11	▽	Polycrystalline Zn foil	0.1 $KHCO_3$	2
12	▷	Oxide-derived Cu	0.5 $NaHCO_3$	2
13	▷	Polycrystalline Cu foil	0.5 $NaHCO_3$	2
14	▷	Cu powder (200-300 nm)	0.1 $KHCO_3$	This work
15	◇	Sn powder (100 nm)	0.1 $KHCO_3$	19
16	◁	MoS_2 powder	$EMIMBF_4$	28
17	□	NCNTs	0.1 $KHCO_3$	This work

Figure 3. Comparison of overpotential and yield of CO of NCNTs with metal catalysts. For Au, Ag, and MoS_2 catalyst, the lowest overpotential is chosen to reach a comparable FE of CO of around 80%. For Zn, Cu, and Sn catalyst, the overpotential for the maximum FE of CO is used.

The CO starts to be formed with a Faradaic efficiency (FE) of 37% at an applied cell potential as low as −0.70 V, which corresponds to an overpotential of −0.18 V with respect to the apparent standard cell potential of −0.52 V for CO_2 reduction to CO in the electrolyte of 0.1 M $KHCO_3$ (Figure 2b).[19] NCNTs display lower onset overpotential and higher correspondent FE of CO than that for Ag nanoparticles (−0.27 V with FE of CO 17%) and Au powder (−0.27 V with FE of CO 12%) under identical testing conditions (Supporting Information, Figures S4 and S5). This onset overpotential is also lower than that recently reported using carbon nanofibers (−0.23 V) mediated by ionic liquid of 1-ethyl-3-methylimidazolium tetrafluoroborate (EMIM−BF_4).[20] The maximum FE of CO reaches around 80% at −0.78 V, which also corresponds to a low overpotential of −0.26 V. The achievable maximum FE of CO for NCNTs is comparable to that for Ag nanoparticles and Au powder; however, the overpotential to reach this highest FE of CO is far lower for NCNTs compared to noble metal Ag and Au catalysts, which means more energy efficient for NCNTs than Ag and Au (Supporting Information, Figures S4 and S5). We further compared the least overpotential required for Ag and Au catalysts in the literatures to reach the comparable FE of CO of around 80% with that of NCNTs (Figure 3). The overpotentials for the highest FE of CO for metal catalysts such as Sn, Zn, and Cu are also included in the Figure 3 for comparison (see details in ref 19 for Sn, Supporting Information, Figure S6, for Zn, and

Supporting Information, Figure S7, for Cu). To reach 80% FE of CO, NCNTs show much lower overpotential than most of the Ag and Au electrodes except oxide-derived Au nanoparticles and ionic liquid mediated Ag powder.[1,5] These two cases are distinct from conventional polycrystalline metal catalysts with aqueous electrolyte. Oxide-derived Au electrode composed of 20−40 nm Au nanoparticles exhibits enhanced CO_2 reduction activity compared to the polycrystalline Au electrode possibly due to the presence of highly active sites on its grain boundary surfaces, similar to oxide-derived Cu electrodes.[21] The enhancement of activity for Ag powder is attributed to the presence of ionic liquid EMIM−BF_4 that complexes with the $(CO_2)^-$ intermediate to lower the initial reduction barrier.[5]

As a benchmark, we also performed CO_2 reduction on pristine CNT arrays. These CNT arrays have been synthesized by benzene as C precursor and ferrocene as catalyst precursor as reported in our previous publication (Supporting Information, Figures S8−S10).[22] These CNTs show poor activity toward CO_2 reduction. The formation of CO starts at a cell potential of −1.38 V that is more negative than that for NCNTs. Moreover, the FE of CO is around 3.5% at this potential, much lower than that for NCNTs (Figure 2b). In addition to CO, formate is detected for CO_2 reduction on CNTs but has a low yield, similar to that of CO, with an FE around 2.0−3.5% in the applied potential range of −1.38 to −2.10 V. The effect of trace metal (*i.e.*, Fe in our case) on the catalytic activity toward ORR is an issue under debate. Actually, Fe has been proven to have no activity toward CO_2 reduction, resulting in H_2 evolution of ∼100% in Faradaic efficiency.[23] In our case, we have intentionally chosen the CNTs sample containing relatively higher Fe residuals than NCNTs, as evidenced by the higher current density of Fe residual redox peaks in the CV performed in a glassy carbon electrode (Supporting Information, Figure S11). The much lower activity of CNTs than NCNTs suggests the active sites are mainly attributed to N-doping rather than the Fe residuals.

Partial current density for CO production (j_{CO}) as a function of potential was extracted from data for the constant potential electrolyses (Figure 2c). The j_{CO} for NCNTs is 1 order of magnitude higher than that for CNTs. The huge difference in activity between CNTs and NCNTs indicates the significant role of N dopant playing in the electrocatalysis process. The CO_2 reduction kinetics is facilitated as the cell potential sweeps cathodically leading to the increase of j_{CO} for NCNTs. The j_{CO} for NCNTs undergoes a plateau as the cell potential shifts more negatively beyond overpotential −0.41 V, reflecting mass transport limitation of CO_2 to the electrodes (Figure 2c). The FE of CO decreases after the achievement of mass transport limitation because more electrons are consumed by HER than CO_2 reduction reaction (Figure 2b).

The stability is equally important to the activity when developing catalysts for CO_2 reduction. Severe degradation occurs to the metal catalysts, like Cu and Au, and so far, the mechanism is still obscure.[1,2,24] Thus, we tested the long-term performance of NCNTs catalysts at constant cell potential of −0.8 V for 10 h. The current density maintains a steady value at around −1.0 mA cm^{-2} throughout the duration of the test. Moreover, the FE of CO only fluctuates slightly around 80% over the test duration. After the long-term running, we analyzed the morphology and surface chemistry of the NCNTs electrode. The NCNTs keep the bamboo morphology after electrolysis of 10 h (Supporting Information, Figure S12). In the electrolyzed electrode, the respective concentration for pyridinic, pyrrolic, and graphitic N is 1.4%, 1.3%, and 2.0 atom%, which falls into the statistic region of N composition for the fresh electrodes, showing the robustness of NCNTs electrodes under reduction condition (Supporting Information, Figure S12). These results clearly reveals that NCNTs act as highly active and durable catalysts for the electrochemical conversion of CO_2 to CO.

In order to understand the mechanism of electrocatalytic CO_2 reduction to CO with such a superior activity for NCNTs in terms of high efficiency and selectivity, the following three questions are open to be answered. (1) Why does the pathway only produce CO, without any hydrocarbons and alcohols? (2) Why is such a small overpotential in electrocatalysis of CO_2 reduction to CO possible? (3) Why do the NCNTs reduce CO_2 to CO with a high yield/Faradaic efficiency? We proposed a mechanism to address the above three questions based on computational hydrogen electrode (CHE) model[29] and density functional theory (DFT) simulations implemented in Vienna Ab-initio Simulation Package (VASP).[30] The answers to these questions should also shed light on modification of carbon nanostructures to further improve the activity.

We consider the reaction mechanism of electroreduction of CO_2 to CO on pristine CNT and NCNT surfaces through the adsorbed intermediates COOH* and CO*. Similar intermediates have been proposed for the electroreduction of CO_2 on late transition metals like Au, Pt, and Cu.[29,31] The elemental reaction steps for the CO_2 electrocatalytic reduction to CO are shown in eqs 1−3[31]

$$CO_2(g) + * + H^+(aq) + e^- \leftrightarrow COOH* \quad (1)$$

$$COOH* + H^+(aq) + e^- \leftrightarrow CO* + H_2O(l) \quad (2)$$

$$CO* \leftrightarrow CO(g) + * \quad (3)$$

where * denotes a free step site. This reaction mechanism involves two coupled electron−proton-transfer reaction steps (eqs 1 and 2) and one nonelectrochemical step, CO desorption (eq 3). The corresponding free energy diagram for the lowest energy pathways for

CO_2 reduction to CO through this scheme is shown in Figure 4, which is calculated on the basis of the CHE model (see details of calculations in the Supporting Information).[29,32] The overpotential strongly depends on free energies of the first two electrochemical steps. For NCNTs, the activation of CO_2 to form adsorbed COOH* is associated with an uphill process of the first electron−proton pair transfer at 0 V *versus* RHE. After the adsorption of COOH, the free-energy pathway becomes thermodynamically downhill to transfer the second electron−proton pair to form adsorbed CO. This CO is weakly bound to the NCNT surface (details are discussed in Figure 5a), leading to the production of CO gas. The potential-limiting step is the formation of adsorbed COOH*, requiring an onset potential of −0.30 V *versus* RHE at which the step becomes exergonic (downhill in free energy) at the pyridinic N site. It implies an existence of limiting (least negative) overpotential of −0.20 V which is close to the experimental observation as shown in Figure 2b. The calculated limiting overpotential for pyridinic N is lower than theoretical values for Cu (−0.31 V), Au (−0.63 V), and Ag (−0.79 V).[29,33] The most efficient N configuration is pyridinic N followed by pyrrolic and graphitic N. In the case of CNTs, the potential-limiting step is also the formation of adsorbed COOH* but requiring an overpotential of −1.9 V, much higher than that for NCNTs, which is in agreement with the experimental data as seen in Figure 2b.

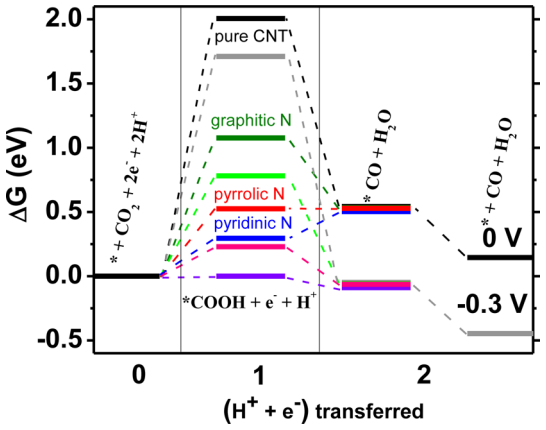

Figure 4. Calculated free energy diagram for CO_2 electroreduction to CO on pristine CNTs and NCNTs. The free energy diagram shows the lowest energy pathway at 0 V *versus* RHE as well as at an applied least negative potential of −0.3 V *versus* RHE at which the pathway becomes exergonic.

Moreover, in order to elucidate the high selectivity of NCNTs toward CO production, we correlated the kinetic activity toward CO production with the adsorption energies of COOH ($E_{B[COOH]}$) and CO ($E_{B[CO]}$).[31,33] Essentially, a highly selective catalyst for CO_2 reduction to CO is required to possess the capability of immobilizing COOH but loosening CO at the same time. In other words, it requires strong COOH binding but a weak CO adsorption. The $E_{B[COOH]}$ and $E_{B[CO]}$ for pristine and different N functionality-doped CNTs were calculated (see details in the Supporting Information), and the results are shown in Figure 5a. The data of metal catalysts from ref 33 are also included in Figure 5a. For the elemental metal catalysts, the $E_{B[COOH]}$ and $E_{B[CO]}$ are linearly correlated with a small positive slope less than one (around 0.73), which suggests that increasing the bonding strength of COOH to the metal surface is accompanied by a sharp increase of CO adsorption energy. Therefore, all elemental metals are off the maximum of kinetic activity to electroreduce CO_2 to CO. For the CNTs materials, the ΔE_{COOH} *versus* ΔE_{CO} is also positively linear. However, the slope for the linear relationship has a much larger magnitude of around 37, and thus, a significant increase of $E_{B[COOH]}$ only causes a slight increase of $E_{B[CO]}$ in NCNTs, which fulfills the essential requirement for a highly selective catalysts for CO evolution. The binding energy profile indicates the highest selective site toward CO production is pyridinic N followed by pyrrolic and graphitic N. The pyridinic N has a very negative value of $E_{B[COOH]}$ as reactive metals like Pt and Ni so that COOH can bind tightly. On the other hand, it has a weak $E_{B[CO]}$ similar to Au and Ag, which renders the feasible desorption of adsorbed CO*. Both pyrrolic and graphitic N are also calculated to have stronger $E_{B[COOH]}$ and weaker $E_{B[CO]}$ than the most CO-selective elemental metal catalysts

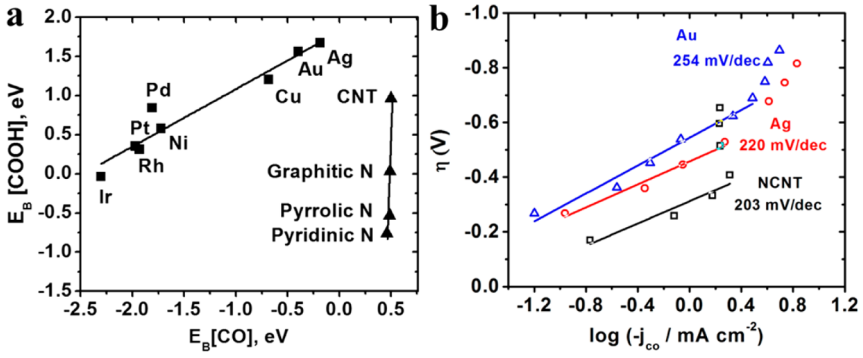

Figure 5. Kinetic activity of NCNTs and metal catalysts. (a) Correlation of calculated adsorption energies of the key bound intermediates of COOH* and CO*. The binding energy data for lattice surface (211) of metals are adopted from ref 33. (b) Experimental Tafel plots of NCNT, Au, and Ag electrodes.

like Au and Ag. As a result, the gas product of CO is favorably produced on NCNTs instead of hydrocarbons and alcohols, as CO is released easily from active N sites on NCNTs before it can be further reduced by the successive electrons. The binding energy profile of COOH and CO for the three N configurations provides insight into the high FE of CO up to 80% for NCNTs in our measurements. For the CNTs, although the binding energy for both COOH and CO are reasonable for selective CO production, the free energy barrier for the first electron−proton pair transfer is too high resulting in a very high onset overpotential at which the HER is also promoted and predominates over CO_2 reduction. Therefore, CNTs exhibit a low yield of CO.

In order to further verify the validation of the adsorption energy plot, a comparison of the kinetic data extracted from the Tafel plots, $\log(j_{CO})$ *versus* overpotential (η), was made among NCNTs, Au, and Ag (Figure 5b). The NCNTs show the smallest Tafel slope (∼200 mV/dec) compared to Au and Ag in the low overpotential regime of −0.17 ∼ −0.41 V. Additionally, the NCNTs possess exchange current density for CO production, obtained from the extrapolation of the Tafel region to reversible potential, three times as big as Au and Ag (Supporting Information, Table S1). The experimental kinetic data match well with the theoretical prediction of superior activity of NCNTs toward CO formation over metals Au and Ag.

CONCLUSIONS

In summary, we have synthesized heavily nitrogen-doped carbon nanotube arrays with total N content of 5 atom % by liquid CVD method. The NCNT array acts as a highly active, selective, and stable catalyst for electrocatalytic reduction of CO_2 to CO. Compared to noble metals Au and Ag, these NCNTs exhibit lower overpotentials to achieve the similar selectivity toward the production of CO. The maximum FE of CO reaches around 80% at a low overpotential of −0.26 V. In contrast, pristine CNTs show poor activity and selectivity toward electroreduction of CO_2. The superior activity for NCNTs is mainly attributed to a low free energy barrier for the potential-limiting step to form adsorbed COOH. Moreover, the suitable binding energy of the key intermediates enables strong COOH adsorption and feasible CO desorption that contributes to the high selectivity toward CO formation. We propose that economical NCNTs are successful alternatives to expensive noble metal electrocatalysts for commercial CO_2 reduction application, with the promise of more efficiency and higher selectivity.

METHODS

Material Synthesis. The NCNTs were synthesized by liquid chemical vapor deposition (CVD) method injecting liquid precursor acetonitrile and dicyandiamide with ferrocene in Ar/H_2 atmosphere at 850 °C. The concentration of ferrocene in precursors kept at 5 mg mL^{-1}. The quartz tube with diameter 5 cm and length 1 m was placed in a three-zone horizontal furnace with the heating zone of 81 cm. The furnace was heated to the desired temperature from room temperature under the argon ambience. When the optimum temperature was reached, the precursors were injected by the syringe pump in the quartz tube with a flow rate of 12 mL h^{-1} in Ar/H_2 (80:20) atmosphere with a flow rate of 1000 SCCM. After the experiment, the furnace was cooled in Ar atmosphere. The pristine CNT arrays were synthesized by injecting benzene and ferrocene solution under growth conditions similar to those for NCNTs. The details about the experimental procedure are given in our previous papers.[22,34]

Catalyst Characterization. The morphology of the materials were characterized by scanning electron microscope (SEM, FEI Quanta 400 FEG ESEM) and high-resolution field emission gun transmission electron microscope (TEM, JEOL 2100 FEG TEM). The crystallinity was measured by powder X-ray diffraction (XRD) collected by Rigaku D/Max Ultima II. The microstructure was studied by Raman spectra using Renishaw inVia Raman microscope with 514 nm laser excitation. The chemical composition was investigated by X-ray photoelectron spectroscopy (XPS, PHI Quantera XPS) on a PHI-5000C ESCA system with Al Kα X-ray as an excitation source.

Electrochemical Measurements. The details of NCNT gas diffusion electrode (GDE) preparation are given in the Supporting Information. The geometric surface area of GDE was 3.8 cm^2. The loading of NCNTs was around 0.5 mg cm^{-2}. The electrochemical test was carried out in a custom-designed full electrochemical cell with NCNT GDE as the cathode electrode, Pt GDE as the anode electrode, and 0.1 M $KHCO_3$ as the electrolyte. The cell runs at room temperature and ambient pressure. The cyclic voltammetry was carried out in the potential range of 0.15 to −1.0 V. The CO_2 reduction was conducted under potentiostatic mode for 30 min at each potential by employing a potentiostat/galvanostat (Solartron 1470E). All of the cell potentials were corrected by the IR drop. The Ohmic resistance of the full electrochemical cell was measured from the electrochemical impedance spectroscopy at open circuit voltage, with an amplitude of 5 mV and frequency range from 100 kHz to 0.1 Hz.

Product Quantification. Gas products from the outlet of the cathodic compartment were vented directly into the gas-sampling loop of the gas chromatograph (GC, Inficon Micro 3000 GC). A GC run was initiated every 10 min. The gas concentration was averaged over three measurements. Liquid products were identified using 1D ^1H NMR spectroscopy (Varian Mercury/VX 400 MHz spectrometer) using the WET solvent suppression pulse sequence. The sodium 3-(trimethylsilyl) propionate-2,2,3,3-d_4 (TSP) was used as the internal standard to quantify the liquid product concentration.

Conflict of Interest: The authors declare no competing financial interest.

Supporting Information Available: Electrode preparation, anode hydrogen evolution potential calibration, DFT calculation, Cu, Ag, Au, and Zn powder for the CO_2 reduction reaction, CNT characterization, and NCNT post-testing characterization. This material is available free of charge *via* the Internet at http://pubs.acs.org.

Acknowledgment. J.W. acknowledges funding support from the U.S. Air Force Office of Scientific Research (Award No. FA9550-14-1-0268). R.M.Y. acknowledges financial support from University Grants Commission, Government of India, for the Raman Fellowship. We also acknowledge financial support from U.S. Air Force Office of Scientific Research (Award No. FA9550-12-1-0035). We thank Dr. Vijayamohanan K. Pillai from the Central Electrochemical Research Institute of India for the valuable comments. The manuscript was co-written by J.W., M.L., and X.Z. All authors participated in the discussion.

REFERENCES AND NOTES

1. Chen, Y.; Li, C. W.; Kanan, M. W. Aqueous CO_2 Reduction at Very Low Overpotential on Oxide-Derived Au Nanoparticles. *J. Am. Chem. Soc.* **2012**, *134*, 19969–19972.
2. Li, C. W.; Kanan, M. W. CO_2 Reduction at Low Overpotential on Cu Electrodes Resulting from the Reduction of Thick Cu_2O Films. *J. Am. Chem. Soc.* **2012**, *134*, 7231–7234.
3. Wu, J. J.; Risalvato, F. G.; Ke, F. S.; Pellechia, P. J.; Zhou, X. D. Electrochemical Reduction of Carbon Dioxide I. Effects of the Electrolyte on the Selectivity and Activity with Sn Electrode. *J. Electrochem. Soc.* **2012**, *159*, F353–F359.
4. Zhang, S.; Kang, P.; Meyer, T. J. Nanostructured Tin Catalysts for Selective Electrochemical Reduction of Carbon Dioxide to Formate. *J. Am. Chem. Soc.* **2014**, *136*, 1734–1737.
5. Rosen, B. A.; Salehi-Khojin, A.; Thorson, M. R.; Zhu, W.; Whipple, D. T.; Kenis, P. J. A.; Masel, R. I. Ionic Liquid-Mediated Selective Conversion of CO_2 to CO at Low Overpotentials. *Science* **2011**, *334*, 643–644.
6. Chen, Z.; Kang, P.; Zhang, M.-T.; Stoner, B. R.; Meyer, T. J. Cu(ii)/Cu(0) electrocatalyzed CO_2 and H_2O splitting. *Energy. Environ. Sci.* **2013**, *6*, 813–817.
7. Jermann, B.; Augustynski, J. Long-term activation of the copper cathode in the course of CO_2 reduction. *Electrochim. Acta* **1994**, *39*, 1891–1896.
8. DeWulf, D. W.; Jin, T.; Bard, A. J. Electrochemical and Surface Studies of Carbon Dioxide Reduction to Methane and Ethylene at Copper Electrodes in Aqueous Solutions. *J. Electrochem. Soc.* **1989**, *136*, 1686–1691.
9. Fan, M.; Bai, Z.; Zhang, Q.; Ma, C.; Zhou, X.-D.; Qiao, J. Aqueous CO_2 reduction on morphology controlled CuxO nanocatalysts at low overpotential. *RSC Adv.* **2014**, *4*, 44583–44591.
10. Kedzierzawski, P.; Augustynski, J. Poisoning and Activation of the Gold Cathode during Electroreduction of CO_2. *J. Electrochem. Soc.* **1994**, *141*, L58–L60.
11. Li, H.; Oloman, C. The Electro-Reduction of Carbon Dioxide in a Continuous Reactor. *J. Appl. Electrochem.* **2005**, *35*, 955–965.
12. Köleli, F.; Atilan, T.; Palamut, N.; Gizir, A. M.; Aydin, R.; Hamann, C. H. Electrochemical reduction of CO_2 at Pb- and Sn-electrodes in a fixed-bed reactor in aqueous K_2CO_3 and $KHCO_3$ media. *J. Appl. Electrochem.* **2003**, *33*, 447–450.
13. Gong, K.; Du, F.; Xia, Z.; Durstock, M.; Dai, L. Nitrogen-Doped Carbon Nanotube Arrays with High Electrocatalytic Activity for Oxygen Reduction. *Science* **2009**, *323*, 760–764.
14. Li, Y.; Zhou, W.; Wang, H.; Xie, L.; Liang, Y.; Wei, F.; Idrobo, J.-C.; Pennycook, S. J.; Dai, H. An oxygen reduction electrocatalyst based on carbon nanotube-graphene complexes. *Nat. Nanotechnol.* **2012**, *7*, 394–400.
15. Kang, P.; Zhang, S.; Meyer, T. J.; Brookhart, M. Rapid Selective Electrocatalytic Reduction of Carbon Dioxide to Formate by an Iridium Pincer Catalyst Immobilized on Carbon Nanotube Electrodes. *Angew. Chem., Int. Ed.* **2014**, *126*, 8853–8857.
16. Zhao, H.; Zhang, Y.; Zhao, B.; Chang, Y.; Li, Z. Electrochemical Reduction of Carbon Dioxide in an MFC−MEC System with a Layer-by-Layer Self-Assembly Carbon Nanotube/Cobalt Phthalocyanine Modified Electrode. *Environ. Sci. Technol.* **2012**, *46*, 5198–5204.
17. Zhang, S.; Kang, P.; Ubnoske, S.; Brennaman, M. K.; Song, N.; House, R. L.; Glass, J. T.; Meyer, T. J. Polyethylenimine-Enhanced Electrocatalytic Reduction of CO_2 to Formate at Nitrogen-Doped Carbon Nanomaterials. *J. Am. Chem. Soc.* **2014**, *136*, 7845–7848.
18. Dresselhaus, M. S.; Jorio, A.; Hofmann, M.; Dresselhaus, G.; Saito, R. Perspectives on Carbon Nanotubes and Graphene Raman Spectroscopy. *Nano Lett.* **2010**, *10*, 751–758.
19. Wu, J.; Risalvato, F. G.; Sharma, P. P.; Pellechia, P. J.; Ke, F.-S.; Zhou, X.-D. Electrochemical Reduction of Carbon Dioxide II. Design, Assembly, and Performance of Low Temperature Full Electrochemical Cells. *J. Electrochem. Soc.* **2013**, *160*, F953–F957.
20. Kumar, B.; Asadi, M.; Pisasale, D.; Sinha-Ray, S.; Rosen, B. A.; Haasch, R.; Abiade, J.; Yarin, A. L.; Salehi-Khojin, A. Renewable and metal-free carbon nanofibre catalysts for carbon dioxide reduction. *Nat. Commun.* **2013**, 4.
21. Li, C. W.; Ciston, J.; Kanan, M. W. Electroreduction of carbon monoxide to liquid fuel on oxide-derived nanocrystalline copper. *Nature* **2014**, *508*, 504–507.
22. Srivastava, A.; Srivastava, O. N.; Talapatra, S.; Vajtai, R.; Ajayan, P. M. Carbon nanotube filters. *Nat. Mater.* **2004**, *3*, 610–614.
23. Azuma, M.; Hashimoto, K.; Hiramoto, M.; Watanabe, M.; Sakata, T. Electrochemical Reduction of Carbon Dioxide on Various Metal Electrodes in Low-Temperature Aqueous $KHCO_3$ Media. *J. Electrochem. Soc.* **1990**, *137*, 1772–1778.
24. Hori, Y.; Konishi, H.; Futamura, T.; Murata, A.; Koga, O.; Sakurai, H.; Oguma, K. "Deactivation of copper electrode" in electrochemical reduction of CO_2. *Electrochim. Acta* **2005**, *50*, 5354–5369.
25. Hori, Y.; Wakebe, H.; Tsukamoto, T.; Koga, O. Electrocatalytic process of CO selectivity in electrochemical reduction of CO2 at metal electrodes in aqueous media. *Electrochim. Acta* **1994**, *39*, 1833–1839.
26. Lu, Q.; Rosen, J.; Zhou, Y.; Hutchings, G. S.; Kimmel, Y. C.; Chen, J. G.; Jiao, F. A selective and efficient electrocatalyst for carbon dioxide reduction. *Nat. Commun.* **2014**, 5.
27. Delacourt, C.; Ridgway, P. L.; Kerr, J. B.; Newman, J. Design of an Electrochemical Cell Making Syngas ($CO + H_2$) from CO_2 and H_2O Reduction at Room Temperature. *J. Electrochem. Soc.* **2008**, *155*, B42–B49.
28. Asadi, M.; Kumar, B.; Behranginia, A.; Rosen, B. A.; Baskin, A.; Repnin, N.; Pisasale, D.; Phillips, P.; Zhu, W.; Haasch, R.; Klie, R. F.; Kral, P.; Abiade, J.; Salehi-Khojin, A. Robust carbon dioxide reduction on molybdenum disulphide edges. *Nat. Commun.* **2014**, 5.
29. Peterson, A. A.; Abild-Pedersen, F.; Studt, F.; Rossmeisl, J.; Norskov, J. K. How copper catalyzes the electroreduction of carbon dioxide into hydrocarbon fuels. *Energy. Environ. Sci.* **2010**, *3*, 1311–1315.
30. Kresse, G.; Furthmüller, J. Efficient iterative schemes for ab initio total-energy calculations using a plane-wave basis set. *Phys. Rev. B* **1996**, *54*, 11169–11186.
31. Hansen, H. A.; Varley, J. B.; Peterson, A. A.; Nørskov, J. K. Understanding Trends in the Electrocatalytic Activity of Metals and Enzymes for CO_2 Reduction to CO. *J. Phys. Chem. Lett.* **2013**, *4*, 388–392.
32. Nørskov, J. K.; Rossmeisl, J.; Logadottir, A.; Lindqvist, L.; Kitchin, J. R.; Bligaard, T.; Jónsson, H. Origin of the Overpotential for Oxygen Reduction at a Fuel-Cell Cathode. *J. Phys. Chem. B* **2004**, *108*, 17886–17892.
33. Peterson, A. A.; Nørskov, J. K. Activity Descriptors for CO_2 Electroreduction to Methane on Transition-Metal Catalysts. *J. Phys. Chem. Lett.* **2012**, *3*, 251–258.
34. Yadav, R.; Dobal, P.; Shripathi, T.; Katiyar, R.; Srivastava, O. Effect of Growth Temperature on Bamboo-shaped Carbon-Nitrogen (C-N) Nanotubes Synthesized Using Ferrocene Acetonitrile Precursor. *Nanoscale Res. Lett.* **2008**, *4*, 197–203.